Conversion of CT numbers into tissue parameters for Monte Carlo dose calculations: a multi-centre study

2007 Phys. Med. Biol. 52 539

(http://iopscience.iop.org/0031-9155/52/3/001)

INSTITUTE OF PHYSICS PUBLISHING PHYSICS IN MEDICINE AND BIOLOGY

Phys. Med. Biol. **52** (2007) 539–562 doi:10.1088/0031-9155/52/3/001

Conversion of CT numbers into tissue parameters for Monte Carlo dose calculations: a multi-centre study

Barbara Vanderstraeten[1], Pik Wai Chin[2], Michael Fix[3], Antonio Leal[4], Grisel Mora[5], Nick Reynaert[1], Joao Seco[6], Martin Soukup[7], Emiliano Spezi[8], Wilfried De Neve[9] and Hubert Thierens[1]

[1] Department of Medical Physics, Ghent University, Gent, Belgium
[2] Velindre Cancer Centre, Department of Medical Physics, Cardiff, UK
[3] Division of Medical Radiation Physics, Inselspital-University of Berne, Berne, Switzerland
[4] Department of Medical Physiology and Biophysics, University of Seville and Virgen Macarena Hospital, Seville, Spain
[5] Nuclear Physics Centre, University of Lisbon, Lisbon, Portugal
[6] Department of Radiation Oncology, Massachusetts General Hospital and Harvard Medical School, Boston, MA, USA
[7] Section for Biomedical Physics, University Hospital Tuebingen, Tuebingen, Germany
[8] Servizio di Fisica Sanitaria, Policlinico S.Orsola Malpighi, Bologna, Italy
[9] Department of Radiotherapy, Ghent University Hospital, Gent, Belgium

E-mail: Barbara.Vanderstraeten@UGent.be

Received 29 September 2006, in final form 22 November 2006
Published 5 January 2007
Online at stacks.iop.org/PMB/52/539

Abstract

The conversion of computed tomography (CT) numbers into material composition and mass density data influences the accuracy of patient dose calculations in Monte Carlo treatment planning (MCTP). The aim of our work was to develop a CT conversion scheme by performing a stoichiometric CT calibration. Fourteen dosimetrically equivalent tissue subsets (bins), of which ten bone bins, were created. After validating the proposed CT conversion scheme on phantoms, it was compared to a conventional five bin scheme with only one bone bin. This resulted in dose distributions D_{14} and D_5 for nine clinical patient cases in a European multi-centre study. The observed local relative differences in dose to medium were mostly smaller than 5%. The dose–volume histograms of both targets and organs at risk were comparable, although within bony structures D_{14} was found to be slightly but systematically higher than D_5. Converting dose to medium to dose to water (D_{14} to D_{14wat} and D_5 to D_{5wat}) resulted in larger local differences as D_{5wat} became up to 10% higher than D_{14wat}. In conclusion, multiple bone bins need to be introduced when Monte Carlo (MC) calculations of patient dose distributions are converted to dose to water.

(Some figures in this article are in colour only in the electronic version)

1. Introduction

In Monte Carlo treatment planning (MCTP), the conversion of computed tomography (CT) numbers into material properties is one of the main factors that determine the accuracy of patient dose calculations (du Plessis *et al* 1998). To interrelate the CT number and the electron density (or stopping power for protons) of a tissue, the CT number scale is often divided into a number of subsets (DeMarco *et al* 1998, Hartmann Siantar *et al* 1997, Ma *et al* 1999, Wang *et al* 1998). Typically, six or fewer different media are defined, e.g. air, lung, fat, water, muscle and bone. Certain Monte Carlo (MC) implementations use a larger number of materials, e.g. MCV (Siebers *et al* 2000a) and the commercial implementation by Nucletron of the VMC++ code (Kawrakow 2001). These systems use over 50 and over 20 materials, respectively. Verhaegen and Devic (2005) have shown that the misassignment of media can lead to large dose errors in MCTP (up to 10% for MV photons). The CT scanner is often calibrated using tissue equivalent materials. However, the elemental composition of those tissue substitutes differs from that of real tissues, resulting in significantly different calibration curves of CT number to electron density (or proton stopping power). For an accurate extraction of tissue properties from CT data, a stoichiometric calibration method was proposed by Schneider *et al* (1996). First, a set of materials (which do not necessarily have to be tissue equivalent) with known elemental compositions and physical densities is scanned to measure the corresponding CT numbers. Next, the results are fitted to a theoretical parameter equation interrelating the CT number and the physical density and atomic number (Z) of each material, at the effective energy of the kV imaging spectrum. Finally, the fitted parameters can be used to calculate the CT numbers of real tissues using tabulated composition data.

The influence of differences in tissue composition on MC dose calculations has been investigated by du Plessis *et al* (1998). They combined the 16 most common human tissue types into dosimetrically equivalent subsets with constant elemental composition by performing MC calculations within homogeneous phantoms. Using a clinical 8 MV photon beam, seven subsets were found to be sufficient to obtain a dose calculation accuracy of 1%. However, for lung and bone further subdivision turned out to be necessary by varying the physical density while keeping the elemental composition constant. The disadvantage of the method of du Plessis *et al* (1998) is that the application of the resulting CT conversion is limited to the beam quality under consideration. Schneider *et al* (2000) therefore proposed a CT conversion method for MC simulations based on the stoichiometric calibration method. Considering 71 human tissues, they created 24 different subsets with constant elemental composition based on the estimated accuracy of the calculated CT numbers.

Instead of converting CT numbers into tissue parameters like elemental composition and mass density, one could also directly extract interaction probabilities from the CT number. This approach is used by the electron MC code VMC (Kawrakow *et al* 1996) and its photon extension XVMC (Fippel 1999). The main advantage is that there is no need to specify any boundaries separating tissue subsets. However, most MC codes explicitly need the elemental composition within each patient voxel to obtain interaction data for dose calculations. Therefore, the VMC/XVMC approach is more difficult to implement in such codes.

The aim of our work was to propose a CT conversion method that is based on the stoichiometric calibration method and that makes use of dosimetrically equivalent tissue subsets based on a clinical 6 MV photon beam, in order to combine the methods of Schneider *et al* (2000) and du Plessis *et al* (1998). Evaluations were performed by means of a MC slab phantom and the Gammex RMI 461A head/body CT phantom using inserts from the Gammex RMI 465 electron density CT phantom (Gammex RMI, Middleton, WI, USA). Furthermore, the effect of selecting a different photon beam quality (15 MV photons) or a different beam

modality (electrons) was investigated. The resulting 6 MV photon binning scheme was compared to a conventional scheme with only five bins. For this purpose a multi-centre study was set up. A stoichiometric CT calibration was performed at seven European centres. Finally, our investigation was focused towards the clinical evaluation of patient treatment plans. Attention was paid to the conversion from dose to medium to dose to water.

2. Materials and methods

2.1. Influence of material composition on photon attenuation and energy deposition

The elemental composition of a material influences dose calculation both through its attenuation and energy deposition characteristics. To determine for which types of human tissue an accurate CT conversion is important and why, mass attenuation coefficients and mass stopping power values were studied for a set of materials (air, water, lung, adipose, muscle, cartilage and cortical bone) as well as for the individual elements that are present within these materials. The attenuation coefficients of the individual elements were taken from the National Institute of Standards and Technology (NIST) photon cross sections (XCOM) database[10] (Hubbell and Seltzer 2004). The mass attenuation coefficient of a mixture can be calculated as the weighted sum of the coefficients of the constituent elements (Jackson and Hawkes 1981). The elemental composition of the human tissues was obtained from ICRU report 44 (ICRU 1989). Mass stopping power values for both the individual elements and human tissues were computed using the NIST electron stopping power and range (ESTAR) database[11].

2.2. Stoichiometric calibration

The following set of materials with known elemental composition was used to calibrate the Siemens Somatom Plus 4 CT scanner at Ghent University Hospital (GUH): PMMA, polystyrene, Gammex RMI solid water, Gammex RMI lung equivalent material and $CaCl_2$ solutions in water of 5, 10, 15, 20, 25, 30 and 35% by weight (maximum solubility around 40%). Table 1 reports their mass density and elemental composition data. A scan protocol used routinely for radiotherapy treatment planning was selected; the tube voltage was 120 kV. For each material the average CT number and standard deviation were determined within a manually drawn region of interest (ROI) on the CT image. Depending on the shape of each material sample, a circular or rectangular ROI was used in order to cover an area as large as possible within the homogeneous material. The stoichiometric calibration procedure of Schneider *et al* (1996) was applied. It makes use of the following empirical formula for parametrization of the total attenuation coefficient μ of a mixture of elements (with elemental weights w_i, atomic numbers Z_i and atomic masses A_i) provided by Jackson and Hawkes (1981):

$$\mu = \rho N_{\mathrm{A}} \sum_{i=1}^{n} \left(\frac{w_i}{A_i} \left(K^{\mathrm{ph}} Z_i^{4.62} + K^{\mathrm{coh}} Z_i^{2.86} + K^{\mathrm{KN}} Z_i \right) \right). \tag{1}$$

In this formula ρ is the mass density and N_{A} is the Avogadro constant. K^{ph} characterizes the cross section of photoelectric absorption, while K^{coh} characterizes the cross sections of both the coherent scattering and the binding correction for the incoherent scattering. K^{KN} represents the Klein–Nishina coefficient. K^{ph}, K^{coh} and K^{KN} depend on the effective energy of the CT

[10] Available online: http://physics.nist.gov/PhysRefData/Xcom/Text/XCOM.html.
[11] Available online: http://physics.nist.gov/PhysRefData/Star/Text/ESTAR.html.

Table 1. Mass density ρ and elemental weights w_i of the set of materials used for the stoichiometric calibration of the Siemens Somatom Plus 4 CT scanner at Ghent University Hospital.

Material	ρ (g cm^{-3})	w_H	w_C	w_N	w_O	w_{Mg}	w_{Si}	w_{Cl}	w_{Ca}
PMMA	1.190	0.081	0.599	0	0.320	0	0	0	0
Polystyrene	1.040	0.077	0.923	0	0	0	0	0	0
Gammex RMI solid water[a]	1.035	0.081	0.673	0.024	0.198	0	0	0.001	0.023
Gammex RMI lung equivalent material[a]	0.300	0.085	0.593	0.020	0.181	0.112	0.008	0.001	0
$CaCl_2$ solution 5%	1.035	0.106	0	0	0.844	0	0	0.032	0.018
$CaCl_2$ solution 10%	1.080	0.101	0	0	0.799	0	0	0.064	0.036
$CaCl_2$ solution 15%	1.126	0.095	0	0	0.755	0	0	0.096	0.054
$CaCl_2$ solution 20%	1.171	0.090	0	0	0.710	0	0	0.128	0.072
$CaCl_2$ solution 25%	1.216	0.084	0	0	0.666	0	0	0.160	0.090
$CaCl_2$ solution 30%	1.261	0.078	0	0	0.622	0	0	0.192	0.108
$CaCl_2$ solution 35%	1.307	0.073	0	0	0.577	0	0	0.224	0.126

[a] As supplied by the manufacturer.

scanner spectrum. The CT number H is expressed in Hounsfield units (HU) and calculated as follows:

$$H = 1000\left(\frac{\mu}{\mu_{\text{water}}} - 1\right). \tag{2}$$

As we only need the attenuation coefficient relative to water to calculate the CT number, only two parameters ($K^{\text{ph}}/K^{\text{KN}}$ and $K^{\text{coh}}/K^{\text{KN}}$) have to be determined by a fit of the measured CT numbers to equations (1) and (2).

The above-mentioned set of calibration materials allowed us to perform a CT scanner calibration for a large range of CT number values through the range of $CaCl_2$ solutions. However, the fact that these solutions need to be fabricated in-house complicated the calibration of CT scanners at other centres. Therefore, a Gammex RMI 465 electron density CT phantom was sent around to perform the stoichiometric calibration. This phantom consists of a 33 cm diameter disc made out of Gammex RMI solid water that includes a matrix of 20 2.8 cm diameter holes. Interchangeable rods of various tissue and water substitutes can be fitted into these holes. For the calibrations 17 different material inserts were used: LN-300 and LN-450 lung equivalent materials, AP6 adipose, polyethylene, breast, CT solid water, CB3 resin, brain, liver, IB1 inner bone, CB4 resin, acrylic, B200 bone mineral, CB2–10% $CaCO_3$, CB2–30% $CaCO_3$, CB2–50% $CaCO_3$ and SB3 cortical bone. Their mass density and elemental composition data were reported by Watanabe (1999). Circular ROIs with a diameter of approximately 2.5 cm were drawn manually on the CT images to determine the average CT number and its standard deviation for each insert. So, the ROIs were approximately the same among the centres. To evaluate the stoichiometric calibration using the Gammex RMI 465 phantom, the phantom was first scanned on the Siemens Somatom Plus 4 CT scanner at GUH and the measured CT numbers for each insert were compared to calculations based on the original stoichiometric calibration (using the set of materials listed in table 1). The same scan protocol was used for both calibrations. Next, the phantom was sent to seven different centres in Europe. A list of the studied CT scanner types and their respective locations can be found in table 2. Each centre used a different scan protocol, depending on the local radiotherapy treatment planning procedure.

Table 2. Results of the stoichiometric calibration using the Gammex RMI 465 electron density CT phantom. All measurements were performed at a tube voltage of 120 kV.

CT scanner	Location	K^{ph}/K^{KN}	K^{coh}/K^{KN}
Siemens Somatom Plus 4	Ghent University Hospital, Belgium	4.24×10^{-5} [a]	-1.77×10^{-3} [a]
Philips Gemini GXL PET/CT	Ghent University Hospital, Belgium	1.99×10^{-5}	9.26×10^{-4}
Siemens Somatom Sensation Open	University Hospital Tuebingen, Germany	2.11×10^{-5}	3.70×10^{-4}
Siemens Somatom Sensation Open	Velindre Cancer Centre, Cardiff, UK	2.30×10^{-5}	3.49×10^{-5}
Siemens Somatom Sensation Cardiac 64	Clinica Quadrantes, Lisbon, Portugal	2.65×10^{-5}	-2.84×10^{-4}
Toshiba Xvision/EX	HUV Macarena, Seville, Spain	3.89×10^{-5}	-8.37×10^{-4}
GE HiSpeed QX/i	Royal Marsden Hospital, London, UK	2.78×10^{-5}	-3.98×10^{-4}
GE ProSpeed	Inselspital Radioonkologie, Berne, Switzerland	1.11×10^{-5}	4.79×10^{-3}

[a] Stoichiometric calibration using the set of materials from table 1 instead of the Gammex RMI 465 phantom.

2.3. Dosimetrically equivalent tissue subsets

After the stoichiometric calibration of each CT scanner, the fitted values of K^{ph}/K^{KN} and K^{coh}/K^{KN} were used to calculate the CT numbers of the 71 human tissues that were also considered by Schneider *et al* (2000, tables 3–5). Mass density and elemental composition data were taken from literature (Woodard and White 1986, White *et al* 1987, ICRU 1989).

The mass density was calibrated continuously in terms of the CT number, as a different value can be assigned to each individual voxel of a MC scoring grid in the BEAMnrc/DOSXYZnrc system (Rogers *et al* 2002). A mass density calibration curve consisting of three separate linear least-squares fits (for air and lung, soft tissues, and bone tissues) was created for each of the CT scanners listed in table 2.

To extract the elemental composition data, the CT number scale was divided into dosimetrically equivalent tissue subsets (bins). To determine the necessary number of subsets, DOSXYZnrc calculations were performed within homogeneous phantoms with dimensions of $31 \times 31 \times 20$ cm^3. The incident beam was a 10×10 cm^2 6 MV photon field produced by the Elekta SL*i*plus linear accelerator at GUH (Van de Walle *et al* 2003). The dimensions of the scoring grid voxels on the central axis were 1 cm in the X and Y directions for all voxels, and 2 mm (voxels 1–20), 4 mm (voxels 21–25) and 1 cm (voxels 26–39) in the Z direction. For each voxel on the central axis, our aim was to keep the maximum deviation between the depth dose curves calculated within two materials representing adjacent tissue subsets below 1%. The statistical uncertainty (1σ) of the MC calculations was less than 0.5% within each voxel on the central axis. Depth dose curves were calculated for air, lung, soft tissues and bone tissues. Each tissue subset was represented by the elemental composition that corresponds with the mean CT number of the subset. As suggested by Schneider *et al* (2000), the elemental composition of human adipose, muscle or bone tissues can be interpolated in good approximation between either adipose tissue 3 and adrenal gland, GI tract and connective tissue, or bone marrow and cortical bone, depending on the CT number. Starting from a conventional five bin scheme (air, lung, adipose, muscle and bone), additional bins were inserted and the corresponding depth dose curves were calculated until the above-mentioned accuracy requirement was fulfilled. To eliminate the influence of mass density on the determination of the number of subsets, it was set to 1 g cm^{-3} for all materials. The number of tissue subsets necessary to achieve dosimetric equivalence within 1% was determined for the Siemens Somatom Plus 4 CT scanner at GUH. An equal number of bins were created for the other CT scanners listed in table 2, taking into account their individual stoichiometric calibration.

To evaluate whether the proposed binning scheme for 6 MV photons is also sufficient for MC calculations using another beam modality and/or a different energy, similar depth dose curves were calculated for the proposed bone subset materials of the Siemens Somatom Plus 4 CT scanner at GUH using a 15 MV photon beam and a 6.6 MeV electron beam (Gaussian energy spectrum with a full width at half maximum value of 0.2 MeV), respectively.

2.4. MC slab phantoms

To evaluate our division of the human bone tissues into a number of subsets, we first performed DOSXYZnrc calculations within MC phantoms. Two heterogeneous slab geometries were defined, consisting of a 0.1 cm and a 1 cm thick layer of bone, respectively, embedded within adipose tissue. The phantom dimensions were $31 \times 31 \times 16$ cm^3. The bone layers were located perpendicularly to the Z-axis either between $Z = 5$ cm and $Z = 5.1$ cm depth or between $Z = 5$ cm and $Z = 6$ cm depth. The incident beam was the 10×10 cm^2 6 MV photon field produced by the Elekta SL*i*plus linear accelerator at GUH. The dimensions of the scoring grid voxels on the central axis were 1 cm in the X and Y directions for all voxels, and down to 0.5 mm in the Z direction for the voxels close to the interfaces between the adipose tissue and the bone layer.

The vertebral column was used to represent the bone layer. Its CT number was calculated using the stoichiometric calibration data of the Siemens Somatom Plus 4 CT scanner at GUH; the elemental composition data were taken from White *et al* (1987). For each geometry (with a 0.1 cm or a 1 cm bone layer), depth dose curves were calculated with the bone layer represented according to the new binning scheme (with multiple bone bins) on the one side, and a conventional binning scheme with a single bone bin representing the material composition of ICRU cortical bone (ICRU 1989) on the other side. For both calculations equal values of the mass density were assigned to the bone layer. The value was derived from the calculated CT number using the mass density calibration curve of the Siemens Somatom Plus 4 CT scanner at GUH. The resulting depth dose curves were compared voxel by voxel along the Z-axis as well as by calculating differences in area below the curves within the bone layer.

2.5. Gammex RMI 461A head/body CT phantom

In addition to the MC slab phantoms, the accuracy of our CT conversion procedure was evaluated on the Gammex RMI 461A phantom. This phantom consists of a 33 cm outer diameter annulus made out of RMI solid water with a central hole into which the inserts of the Gammex RMI 465 tissue calibration phantom can be fitted. The following six inserts were used: LN-300 and LN-450 lung equivalent materials, B200 bone mineral, CB2–10% $CaCO_3$, CB2–30% $CaCO_3$ and CB2–50% $CaCO_3$. DOSXYZnrc was used to calculate dose profiles within a large water phantom positioned 100 cm below the source of the Elekta Precise linear accelerator. The incident beam was a 6 MV photon field with dimensions of 10×10 cm^2 at the phantom surface. The Gammex RMI 461A phantom was placed just below the water surface and the dose profiles were determined along the X-axis at depths of 12 cm and 15 cm below the phantom. The phantom was scanned on the Siemens Somatom Plus 4 scanner at GUH with the different inserts specified above. For each insert, the average CT number was determined within a manually drawn circular ROI with a diameter of approximately 2.5 cm. Next, the CT number was converted into a homogeneous material composition and mass density. Two sets of DOSXYZnrc calculations were performed, one using the material properties derived from our CT conversion and another by modelling the phantom with the exact material properties.

The dimensions of the scoring grid voxels along the calculated dose profiles were $0.25 \times 1 \times 4$ cm^3.

2.6. Patient dose calculations

Finally, our CT conversion procedure was evaluated on patients. Nine patient cases were selected at four different centres (patient numbers 1, 2–3, 4–6 and 7–9, respectively), of which three oropharyngeal cancer patients (patient numbers 1, 3 and 8), three laryngeal cancer patients (5, 6 and 9), one lung cancer patient (2), one breast cancer patient (4) and one patient with a brain tumour (7). Patients 7 and 8 were treated using a 3D conformal treatment technique, while patients 1–3, 4–5 and 9 received intensity-modulated radiation therapy (IMRT) treatment. For the breast cancer patient a single field was evaluated. The selection of patients was based on the presence of bony structures close to or within the high dose region, since this is what our CT conversion focuses on as will be explained in section 3.1. For each patient two MC calculations were performed: the material composition of every voxel was determined once applying the proposed CT conversion scheme and once using a conventional five bin scheme. This five bin scheme was derived from the proposed 14 bin scheme by keeping the first four bins and replacing bins 5–14 by a single bin representing the material composition of ICRU cortical bone. The mass density was derived directly from the CT number in the same, continuous manner for both sets of calculations. In this way two dose distributions were generated for each patient, which will further be referred to as D_{14} and D_5. Dose difference maps (DD) were created by calculating the local relative difference in dose between D_{14} and D_5. Values of DD were only assigned to voxels for which the local value of D_{14} was higher than 50% of the isocentric value of D_{14}. This was done to avoid the occurrence of large local relative dose differences corresponding to small absolute dose differences within the low dose regions, which are not clinically relevant and may thus lead to misinterpretation. Additionally, dose–volume histograms (DVHs) of the relevant target structures and organs at risk were created for each patient.

Whereas conventional dose calculations for photon beam treatment planning report dose to water, MC dose engines calculate dose to medium. When comparing MC results with results obtained by conventional systems, the MC dose distributions must thus be converted to dose to water. Additionally, dosimetry calibration protocols are generally based on absorbed dose to water standards. Although it would be possible to convert measurements and conventional dose results to dose to medium, the most important reason for converting dose to medium to dose to water is that tumour control probability (TCP) and normal tissue complication probability (NTCP) data are usually given in terms of dose to water and it will take a lot of effort and time before biological data can be made available in terms of dose to medium. Liu and Keall (2002) have elaborated on this issue in a point–counterpoint discussion.

Siebers *et al* (2000b) have proposed a method to convert dose to medium to dose to water by applying Bragg–Gray cavity theory. They have shown that a single correction factor can be used for each material—as long as it is not air—throughout the field for a given photon energy. Their post-processing method proved to be equally valid as performing the conversion online during the MC simulations. We have computed the conversion factor for each material of the proposed CT conversion scheme of each CT scanner as the ratio of the water and medium mass stopping powers at an effective electron energy of 1 MeV. As will be shown in section 3.1 and figure 2, the conversion factor of cortical bone amounts up to almost 1.13, while the conversion factors for lung and soft tissues differ by only 1 or a few % from 1, respectively. Hence, large errors may arise when converting dose to medium to dose to water

if the wrong bone composition is assigned. To evaluate the effect of possible conversion errors caused by taking into account an insufficient number of bone bins in a clinical situation, we have converted the above-mentioned MC dose distributions D_{14} and D_5 of each of the nine selected patient cases from dose to medium to dose to water. The converted dose distributions are referred to as D_{14wat} and D_{5wat}. Dose to water difference maps (DD_{wat}) were created by calculating the local relative dose difference between D_{14wat} and D_{5wat}, but values were only assigned to voxels for which the local value of D_{14} was greater than 50% of the isocentric value of D_{14}. Again, DVHs of the relevant target structures and organs at risk were created for each patient.

Finally, to illustrate the influence of using a wrong CT conversion scheme (e.g. from another CT scanner) on patient dose calculations, an additional oropharyngeal patient case treated using a 3D conformal technique was selected. Two CT scanners were chosen from table 2 based on the differences between their mass density calibration curves: the Siemens Somatom Plus 4 CT scanner at GUH (A) and the Siemens Somatom Sensation Open CT scanner at the University Hospital of Tuebingen (B). For the selected patient MC dose calculations were performed using the proposed 14 bin CT conversion schemes of both CT scanners A and B, resulting in the dose distributions D_A and D_B. These dose distributions were compared by means of isodifference plots in transversal planes.

3. Results and discussion

3.1. Influence of material composition on photon attenuation and energy deposition

Figure 1(a) shows the mass attenuation coefficient of each material relative to that of water as a function of the photon energy in the range of 100 keV to 20 MeV. The attenuation properties of tissues like lung, adipose, muscle and cartilage are more or less water equivalent. However, the curves for air and cortical bone clearly deviate. This is due to the H- and Ca-content of those tissues: figure 1(b) shows the mass attenuation coefficient of the individual elements. Lung tissue contains 10.3% by weight of hydrogen, whereas dry air does not contain any hydrogen. This is the main cause of the discrepancy between the mass attenuation coefficients of lung and air, the latter being about 10% lower than the former. The 'cartilage—high Ca' curve in figure 1(a) illustrates the influence of calcium. This curve was created by setting the calcium content of cartilage to that of cortical bone, i.e. 22.5% by weight, while rescaling the other elemental weights. Additionally, the hydrogen content of cartilage (9.6% by weight) is higher than that of cortical bone (3.4% by weight), which accounts for the remaining shift. Therefore, an accurate conversion of CT numbers into elemental H- and Ca-weights is of high importance, as these weights strongly influence photon attenuation (Seco and Evans 2006). Figure 2(a) shows the water-to-material relative mass stopping power as a function of the electron energy in the range of 100 keV to 30 MeV; values for the individual elements are shown in figure 2(b). The energy deposition depends primarily on the hydrogen content.

For radiotherapy beams with photon energies between 0.1 and 10 MeV the Compton effect is the dominant interaction process. As the probability for Compton interaction is proportional to the electron density of a material, it will depend significantly on the hydrogen content (Seco and Evans 2006). At diagnostic imaging energies, however, the calcium content of a material will strongly increase the importance of the photoelectric and Rayleigh scattering terms because of their strong Z-dependence. Because dose calculations use material property data extracted from CT images, the calcium content may indirectly influence the dose calculations if not properly accounted for when converting CT numbers into electron density. Thus, it

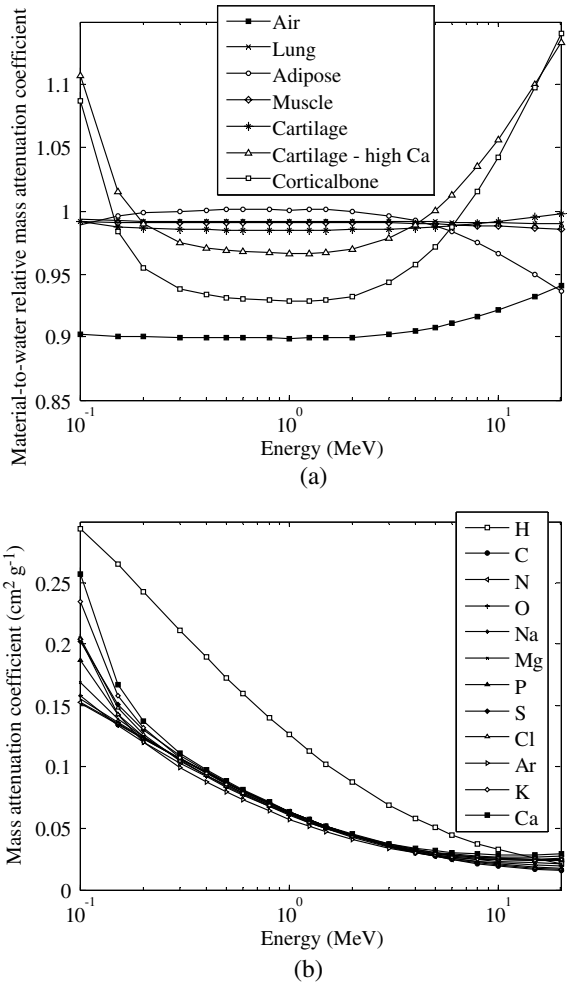

Figure 1. (a) Mass attenuation coefficients of different materials relative to that of water as a function of photon energy (MeV). The 'cartilage—high Ca' curve was created by setting the calcium content of cartilage to that of cortical bone, i.e. 22.5% by weight, while rescaling the other elemental weights. (b) Mass attenuation coefficients of individual elements ($cm^2\ g^{-1}$) as a function of photon energy (MeV).

is particularly important to be able to distinguish lung from air (different H-content) as well as different bone compositions from each other (different H- and Ca-contents) to perform accurate MC patient dose calculations. Magnetic resonance imaging (MRI) techniques may allow us to visualize the H-content within patients, e.g. throughout the lungs. However, the resulting images are generally characterized by a low signal-to-noise ratio and poor resolution. At present, the most practical approach seems to be the selection of a different CT number boundary between air and lung depending on the tumour site, i.e. lower for lung tumours (to assign lung to patient voxels with low CT numbers) and higher for head and neck tumours (to avoid the assignment of lung to patient voxels with low CT numbers, which is anatomically impossible). This matter will not be examined any further in this paper. Instead, our CT conversion procedure will focus on the division of the human bone tissues into a sufficient number of subsets.

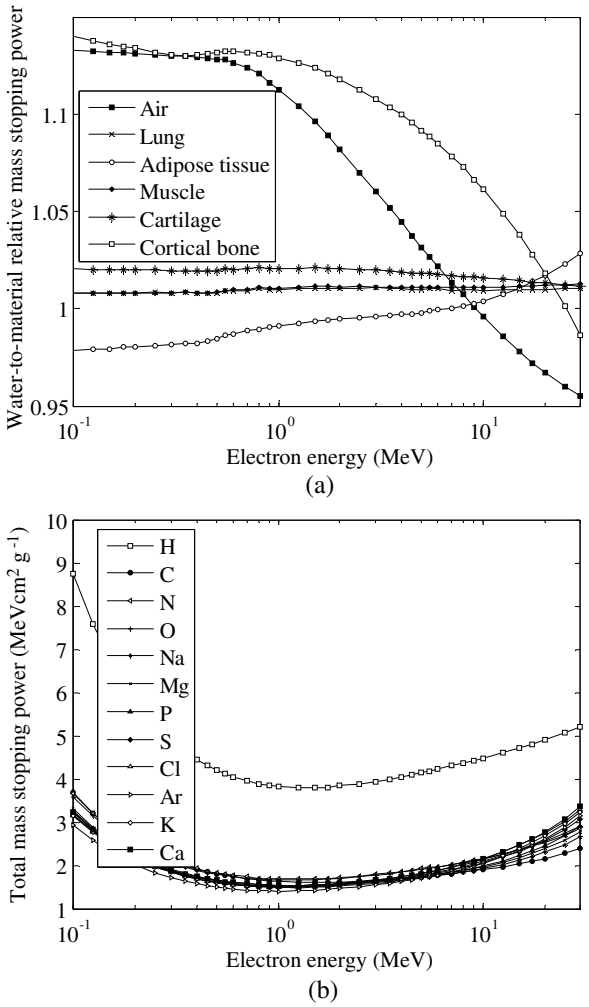

Figure 2. (a) Mass stopping power of water relative to that of different materials as a function of electron energy (MeV). (b) Mass stopping powers of individual elements (MeV cm^2 g^{-1}) as a function of electron energy (MeV).

3.2. Stoichiometric calibration

A fit of the measured CT number data to equations (1) and (2) for the set of materials listed in table 1 resulted in values of $K^{\mathrm{ph}}/K^{\mathrm{KN}}$ and $K^{\mathrm{coh}}/K^{\mathrm{KN}}$ of 4.24×10^{-5} and -1.77×10^{-3}, respectively, for the Siemens Somatom Plus 4 CT scanner at GUH. The R^2-value of the fit was 0.999. The occurrence of a negative value for $K^{\mathrm{coh}}/K^{\mathrm{KN}}$ has been addressed by de Kock and Schreuder (1996). In his reply, Schneider has suggested repeated air calibration measurements and separate scans for each material to obtain a positive K^{coh}. We performed all scans in a clinical setting, i.e. in the same circumstances as for real patients. In any case, the negative K^{coh} yields excellent results. The possibility of decreasing the number of fitting parameters to avoid the occurrence of a negative K^{coh} value is discussed in an appendix to this paper.

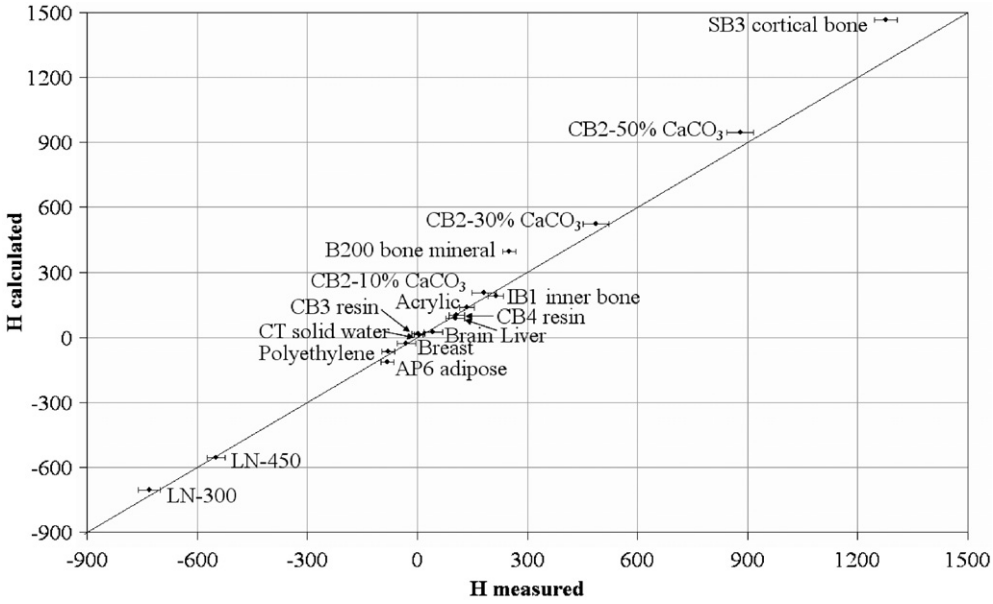

Figure 3. Calculated versus measured CT numbers for the inserts of the Gammex RMI 465 phantom listed in section 1.2 for the Siemens Somatom Plus 4 CT scanner at Ghent University Hospital. Calculations were performed using the stoichiometric calibration based on the set of materials from table 1. The half width of each error bar is equal to one standard deviation of the measured CT number.

Figure 3 shows calculated versus measured CT numbers for the inserts of the Gammex RMI 465 phantom for the same CT scanner. The calculations were performed using the stoichiometric calibration curve based on the set of materials from table 1. The R^2-value of the 1:1 fit was 0.983. The largest deviations occur for B200 bone mineral, CB2–50% $CaCO_3$ and SB3 cortical bone (and to a lesser extent for AP6 adipose). AP6 adipose and B200 bone mineral are the only material inserts containing fluorine (3.1% and 16.7%, respectively), while CB2–50% $CaCO_3$ and SB3 cortical bone are the inserts with the highest calcium content (20.0% and 27.0%, respectively).

Verhaegen and Devic (2005) have already pointed out problems with the use of tissue substitutes containing fluorine, e.g. Teflon, to perform CT calibrations for MC dose calculations. None of the human body tissues contain fluorine. On the other hand, the stoichiometric calibration procedure should be able to accurately predict the CT number of every material with a known composition, on the condition that equation (1) is a valid approximation. The difference between the attenuation coefficient of elemental fluorine calculated through this equation and the value of the same coefficient according to the NIST database (Hubbell and Seltzer 2004) is about −1.5% for an effective CT scanner energy around 70 keV, which cannot account for the large discrepancies observed in figure 4. Possibly there is a difference between the elemental composition data of our calibration materials and the data available in the literature.

The inaccuracy of attenuation coefficients of materials containing considerable amounts of calcium calculated through equation (1) has been reported by de Kock and Schreuder (1996). Schneider *et al* (2000) have provided an interpolation formula for the CT number of a medium that is composed of only two components. We used this formula to compute additional 'measurement' data for artificial $CaCl_2$ and $CaCO_3$ solutions with a high calcium

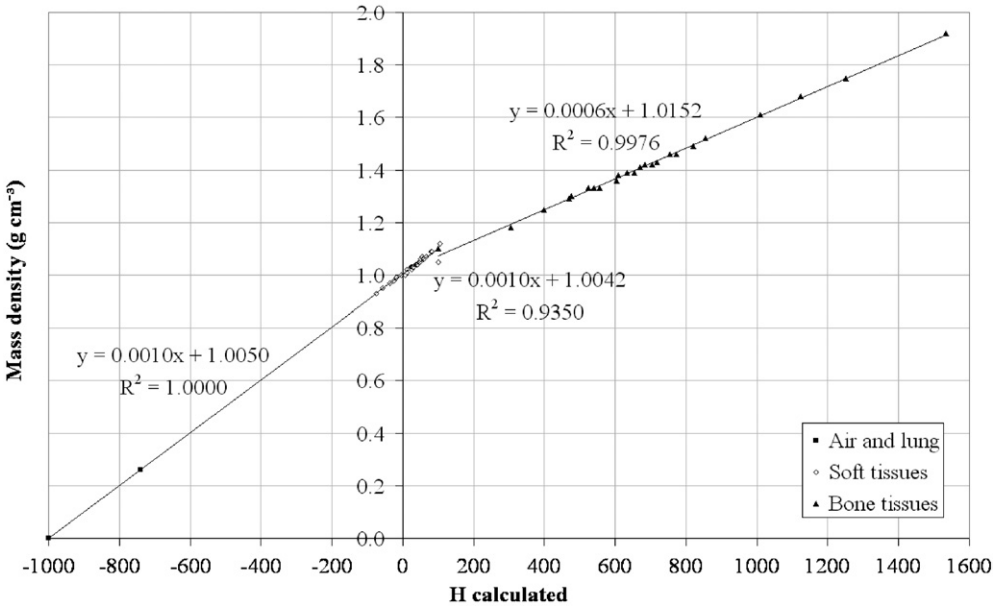

Figure 4. Mass density calibration curve of the Siemens Somatom Plus 4 CT scanner at Ghent University Hospital. The equation of each linear regression curve is displayed as well as the corresponding correlation coefficient.

content (up to 40% by weight). From a comparison between these interpolated and the calculated (using the stoichiometric calibration curve based on the set of materials from table 1) CT numbers it was clear that equation (1) overestimated the CT number for materials with a high calcium content. Moreover, the deviations increased as the calcium content became higher. For materials with w_{Ca} greater than 20%, the R^2-value of the fit was equal to 0.711. The difference between the attenuation coefficient of elemental calcium calculated through equation (1) and the value of the same coefficient according to the NIST database (Hubbell and Seltzer 2004) is about 4.1% for an effective CT scanner energy around 70 keV, while the observed discrepancies were clearly larger.

We extended the equation used to predict CT numbers from material properties with two purely empirical fitting parameters a and b, in addition to K^{ph}/K^{KN} and K^{coh}/K^{KN}. We thus allowed a linear decrease of the calculated CT number with respect to the CT number calculated according to the original equation, for materials with w_{Ca} greater than 20%: $H = (1 - a)H_{original} + b$. In this way, an excellent correspondence between calculated and measured CT numbers could be obtained for these materials ($a = 0.297$, $b = 242$, $R^2 = 0.996$). Only for the artificial $CaCO_3$ solution containing 40% by weight of calcium the result still was not satisfactory. However, the maximum calcium content of even the most dense human bone is at most 30%. We investigated the dosimetric relevance of this empirical extension by calculating the CT number for 27 human bone tissues based on both the original and the extended fit. We determined the corresponding tissue bins according to the binning scheme based on the original fit, which will be presented in section 3.3. For 23 tissues the bin number was the same; for the other four tissues the difference was 1 bin. As the dose difference between adjacent bins is less than 1%, we conclude that the empirical extension of the calibration equation was not dosimetrically relevant. Hence, the observed differences between calculated and measured CT numbers for materials with a high calcium content are acceptable for our purposes.

The Gammex RMI 465 phantom was sent around to different centres to perform a stoichiometric calibration of the CT scanner. Because of the observed discrepancies between the calculated and measured CT numbers of the inserts containing fluorine (AP6 adipose and B200 bone mineral), these data were omitted to fit the measured data to equations (1) and (2). The resulting values of $K^{\mathrm{ph}}/K^{\mathrm{KN}}$ and $K^{\mathrm{coh}}/K^{\mathrm{KN}}$ are listed in table 2. This table illustrates the variety in stoichiometric calibration results found for the investigated scan protocols at different centres. It is absolutely necessary to perform an individual stoichiometric calibration for each CT scanner and scan protocol used for radiotherapy treatment planning. The same scan protocol has to be selected to calibrate the CT scanner and to scan patients. If several scan protocols are used depending on the tumour site, several CT conversion schemes will need to be created at each institution, as different values of the fitted parameters will occur for the same CT scanner using different protocols.

3.3. Dosimetrically equivalent tissue subsets

The mass density calibration curve for the Siemens Somatom Plus 4 scanner at GUH is shown in figure 4. Compared to air/lung and bone, the fit for the soft tissues is clearly worse. This is due to the limited ability to distinguish soft tissues by means of their CT number in the range between 0 and 100 HU as shown by Schneider *et al* (2000), figure 3. It appears that the first two linear regression curves could be combined into a single curve representing air, lung and soft tissues together. Because the individual fits were performed separately, there is a discontinuity between the regression curves of soft and bone tissues. Its effect was evaluated through the comparison of depth dose curves calculated within homogeneous phantoms, corresponding to the soft and bone tissues just left and right of the discontinuity at $H = 100$, respectively. The maximal deviation was equal to 1.07% found at 0.3 cm depth. Therefore, the potential misassignment of a voxel with a CT number close to 100 HU to the last soft tissue bin or first bone tissue bin will not have severe consequences for the performed dose calculations, and the discontinuity between the mass density calibration curves is acceptable.

For the other CT scanners listed in table 2, similar curves were obtained.

The proposed conversion of CT numbers into elemental composition data is presented in table 3 for the Siemens Somatom Plus 4 scanner at GUH. Air and lung were assigned an individual bin each. Two bins were created for soft tissue, i.e. for adipose- and muscle-like tissues. The maximal deviation between the depth dose curves of both subset representatives was 0.97% (found at 2.9 cm depth). Ten equidistant bins were created for bone. The maximal deviation between the depth dose curves of two adjacent subsets was found between the first two bins, and was equal to 1.01% (found at 3.5 cm depth). Based on these findings, 14 tissue subsets were created for each of the CT scanners listed in table 2.

For 15 MV photons, the deviation between the depth dose curves of the first and last bone bin was below 1% at all calculated depths. Indeed, figure 2 clearly shows an intersection between the mass stopping power curves of cartilage and cortical bone at an electron energy of about 20 MeV. Thus, for high energy photon beams used for radiation therapy it will not be necessary to introduce as many bone bins as for low energy beams. The proposed binning scheme can therefore be used for 6 MV beams as well as for higher energies.

For 6.6 MeV electrons, the maximal deviation between the depth dose curves of two adjacent bone bins was found between the first two bins, and was equal to 2.2% (found at 2.3 cm depth), whereas approximately 85% and 95% of all bone bins differ less than 1% and 2%, respectively. The larger than 1% differences are possibly due to a larger effect of electron elastic scattering in the dose deposition for electron beams compared to photon beams. Additionally, there is a large dose gradient at this depth (18.9% mm^{-1} for the depth

Table 3. Proposed conversion of CT numbers into elemental weight data w_i for the Siemens Somatom Plus 4 CT scanner at Ghent University Hospital. H_l and H_u are the lower and upper boundaries of each CT number interval.

H_l	H_u	w_H	w_C	w_N	w_O	w_{Na}	w_{Mg}	w_P	w_S	w_{Cl}	w_{Ar}	w_K	w_{Ca}
	−900			0.755	0.232						0.013		
−900	−100	0.103	0.105	0.031	0.749	0.002		0.002	0.003	0.003		0.002	
−100	20	0.112	0.533	0.011	0.341	0.001			0.001	0.001			
20	100	0.101	0.156	0.040	0.693	0.003		0.001	0.003	0.002		0.001	
100	250	0.095	0.453	0.025	0.355	0.001		0.021	0.002	0.001		0.001	0.046
250	400	0.084	0.401	0.028	0.369	0.001	0.001	0.036	0.002	0.001		0.001	0.077
400	550	0.075	0.355	0.030	0.381	0.001	0.001	0.048	0.002	0.001		0.001	0.105
550	700	0.067	0.316	0.033	0.392	0.001	0.001	0.059	0.002	0.001			0.128
700	850	0.060	0.281	0.035	0.401	0.001	0.001	0.068	0.002				0.149
850	1000	0.053	0.250	0.037	0.410	0.001	0.001	0.077	0.003				0.168
1000	1150	0.048	0.223	0.038	0.417	0.001	0.002	0.084	0.003				0.184
1150	1300	0.043	0.198	0.040	0.423	0.001	0.002	0.091	0.003				0.199
1300	1450	0.038	0.176	0.041	0.429	0.001	0.002	0.097	0.003				0.212
1450		0.034	0.156	0.042	0.435	0.001	0.002	0.103	0.003				0.224

dose curve of the first bone bin), which affects the comparison of the two bone bins. In the first part of the depth dose curve, which is reasonably flat and which is the part that is most relevant to radiotherapy treatment planning, the maximal deviation between the depth dose curves of two adjacent bone bins is again found between the first two bins but only amounts to 0.7%. We therefore consider our proposed CT conversion scheme suitable for photons as well as for electrons. For high energy electrons used for radiotherapy the proposed CT conversion scheme will be satisfactory *a fortiori*, due to the smaller difference between the mass stopping power values of different bone compositions at higher electron energies.

3.4. MC slab phantoms

For the elemental composition of the vertebral column a CT number value of 520 HU was calculated. Thus, the vertebral column would be modelled as the third bone bin by our proposed 14 bin CT conversion scheme (table 3) and as ICRU cortical bone by the conventional five bin scheme. The calculated mass density value was 1.323 g cm^{-3}. Figure 5 shows the resulting depth dose curves for both values of the bone layer thickness (0.1 cm and 1 cm). Local absolute dose differences up to 4.1% (0.1 cm) and 6.4% (1 cm) were observed within the bone layer, and up to 3.3% (0.1 cm) and 4.0% (1 cm) within the adjacent adipose tissue. The differences in area below the depth dose curves within the bone layer were more limited: 2.3% (0.1 cm) and 2.4% (1 cm), respectively.

The calculations for the 0.1 cm thick layer of bone allow us to study energy deposition effects around bony structures embedded within soft tissue, while the calculations for the 1 cm thick layer additionally allow us to study attenuation effects within the bony structure itself. The results indicate that although large dose deviations may be observed locally in or around bony structures within patients, the influence of introducing a larger number of bone bins on integrated dose quantities, e.g. DVHs, is likely to remain limited.

3.5. Gammex RMI 461A head/body CT phantom

Both sets of DOSXYZnrc calculations were compared by averaging the absolute value of the dose difference over the 13 central voxels along the *X*-axis and by normalizing the result using

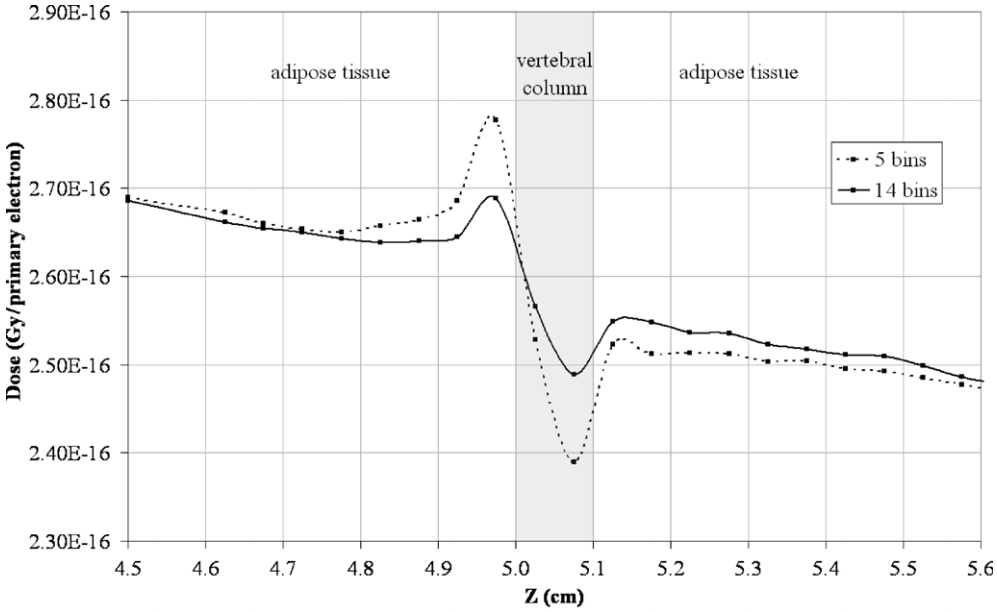

(a)

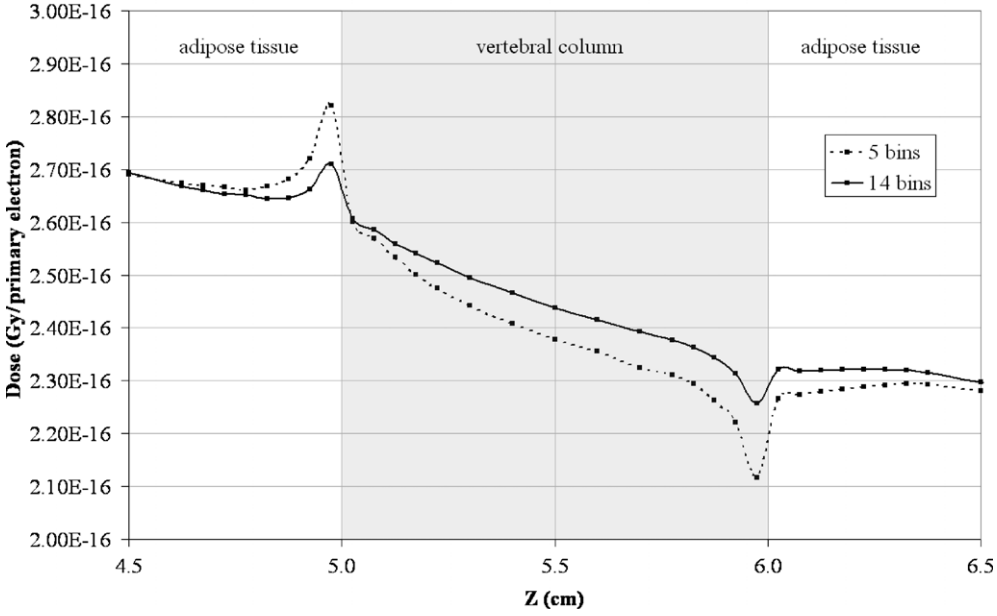

(b)

Figure 5. Depth dose curves within MC slab phantoms consisting of a 0.1 cm (a) and a 1 cm (b) thick layer of vertebral column (520 HU) embedded within adipose tissue. Calculations were performed with the vertebral column layer represented according to a conventional five bin CT conversion scheme (dotted lines) and our proposed 14 bin CT conversion scheme (solid lines) for the Siemens Somatom Plus 4 CT scanner at Ghent University Hospital. The mass density of the bone layer was equal to 1.323 g cm^{-3}.

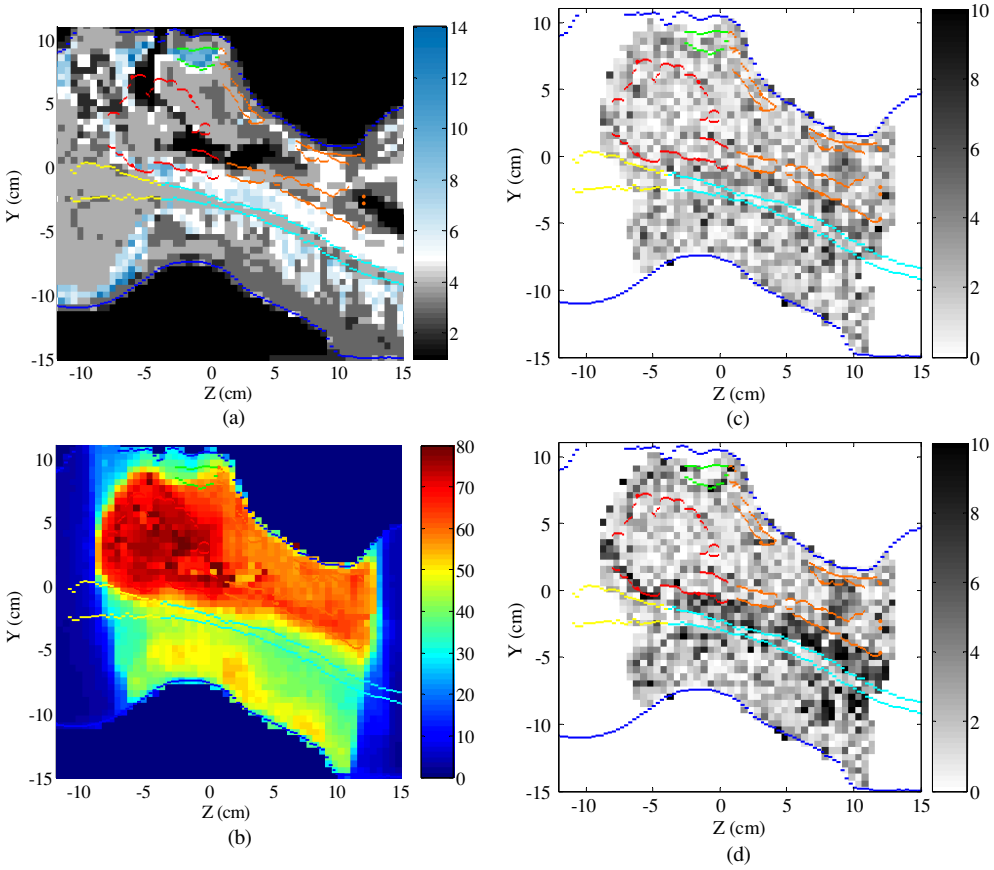

Figure 6. Sagittal views through the isocentre (0, 0, 0) for patient 3, showing the material numbers for the 14 bin conversion scheme (a), the dose distribution D_{14} in Gy (b) and the absolute value (%) of the local dose difference distributions DD (c) and DD_{wat} (d). Contoured structures: PTV_1 (red), PTV_2 (orange), skin (blue), brainstem (yellow), mandible (green) and the spinal cord (cyan).

the average dose calculated within the central voxel. The following results were obtained at 12 cm and 15 cm depth, respectively: 1.0% and 1.1% for LN-300, 0.5% and 0.6% for LN-450, 1.4% and 1.5% for B200 bone mineral, 0.6% and 0.5% for CB2–10% $CaCO_3$, 0.4% and 0.6% for CB2–30% $CaCO_3$ and 0.2% and 0.2% for CB2–50% $CaCO_3$. These numbers confirm the adequacy of our CT conversion procedure. Because the average CT number was converted into a homogeneous material composition and mass density for each insert, the influence of scanning artefacts on the calculations was excluded.

3.6. Patient dose calculations

Figure 6 illustrates the attributed material numbers for the proposed 14 bin conversion scheme for patient 3 in a sagittal slice through the isocentre (a), as well as the D_{14} (b) and DD (c) distributions. The material numbers of the five bin conversion scheme result from the 14 bin conversion scheme by replacing all numbers greater than or equal to 5 by 5. Figure 7 shows DD as a histogram for each patient. It is clear that the observed relative differences between D_{14} and D_5 are spread approximately symmetrically around DD = 0% and are mostly smaller

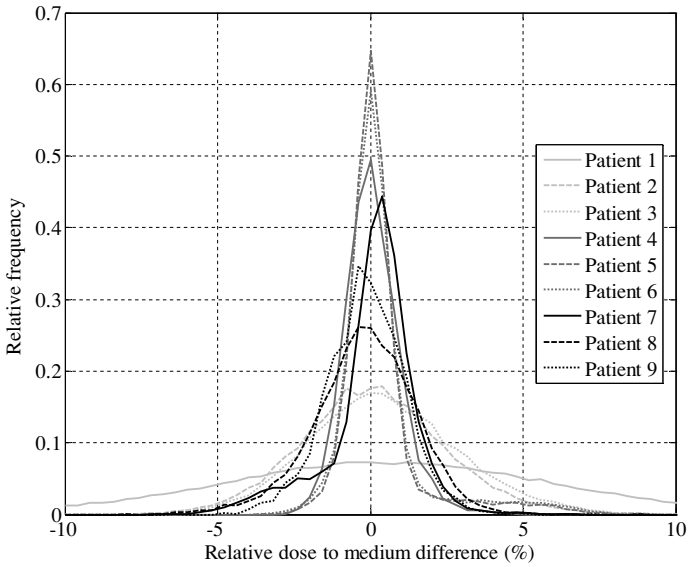

Figure 7. Histograms of the relative dose to medium differences DD (%) between the MC dose distributions D_{14} and D_5, which were calculated based on a 14 bin and a five bin CT conversion scheme, respectively. Each histogram was plotted using a bin width of 0.4%.

than 5%. The largest local dose differences were reported for patient number 1, which was the patient with the smallest voxel size, i.e. $2 \times 2 \times 5$ mm^3. The voxel size of the dose calculation grid was $5 \times 5 \times 5$ mm^3 for patients 2–4, $4 \times 4 \times 3$ mm^3 for patients 5–6 and $4 \times 4 \times 4$ mm^3 for patients 7–9. Despite the observed local differences for each patient, the D_{14}- and D_5-DVHs of the target structures and relevant organs at risk were hardly distinguishable from each other. However, for bony structures like the mandible, maxilla or parts of the PTV for certain patients D_{14} was found to be slightly but systematically higher than D_5. This is due to the higher mass stopping power values of soft bony tissues compared to hard ones like cortical bone as shown in figure 2. Figure 8(a) illustrates the DVHs of D_{14} and D_5 for patient 3.

Table 4 shows the dose to medium to dose to water conversion factors for each material of the proposed CT conversion scheme of the Siemens Somatom Plus 4 CT scanner at GUH. For the other CT scanners listed in table 2, similar tables were obtained. Siebers *et al* (2000b) have associated errors up to 1.3% with these conversion factors, provided that a sufficient number of materials are included in the conversion process (Fippel and Nuesslin 2000, Siebers *et al* 2000c). Figure 6(d) illustrates the dose to water difference distribution DD_{wat} for patient 3 in a sagittal slice through the isocentre. Compared to $DD_{(med)}$ shown in figure 6(c), it is clear that the observed differences were larger, particularly in the bony tissue surrounding the spinal cord. Similar observations were made for the other patients in case of bony structures close to or within the high dose regions, but not for the lung and breast cancer patients.

Figure 9 shows DD_{wat} histograms for each patient. Unlike for DD, there is a distinct asymmetry in the histograms towards negative dose difference values, i.e. D_{5wat} is higher than D_{14wat}. This is due to the fact that for the five bin CT conversion scheme all bony tissues are classified as cortical bone and therefore the dose to water is over 10% higher than the dose to medium within those voxels. For the 14 bin CT conversion scheme, the dose to medium to dose to water correction is only a few % for the first bone bin, while this number quickly rises for the next bone bins. Therefore, possible errors during the conversion from dose to medium

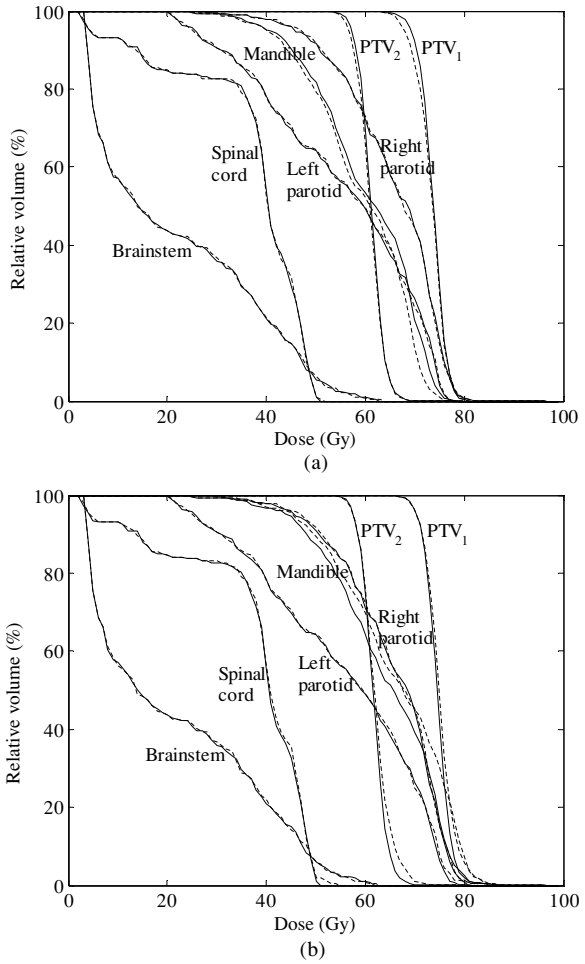

Figure 8. Dose–volume histograms of relevant target structures and organs at risk for patient 3 for D_{14} (solid lines) and D_5 (dashed lines) (a) and for D_{14wat} (solid lines) and D_{5wat} (dashed lines) (b).

to dose to water, caused by considering an insufficient number of bone subsets, will naturally be most apparent within the voxels of which the real composition differs the most from the assigned composition, in our case within the softest bone tissues for the five bin CT conversion scheme. The clear lump around -11% in the DD_{wat} histogram of patient number 9 was caused by the cartilage tissue of the larynx and the spinal cord; for other patients the lumps visible in the histograms were primarily due to the skull (patient 7), the skull base (patients 5, 6 and 8), the mandible (patients 5 and 8) and the spinal cord (patient 5). For patient 1, the large amount of bony tissue present within the high dose region caused a shift of the maximum of the histogram of about 5% towards negative dose difference values.

Although histograms are a good means to visualize the dose difference distribution, attention should also be paid to the clinical significance of the observed differences, i.e. to take into account their location with respect to the tumour and organs at risk. Indeed, if considerable errors are encountered within bony tissue that is not part of or close to any relevant structures there is less cause for concern with regard to the patient's treatment. To evaluate the effect

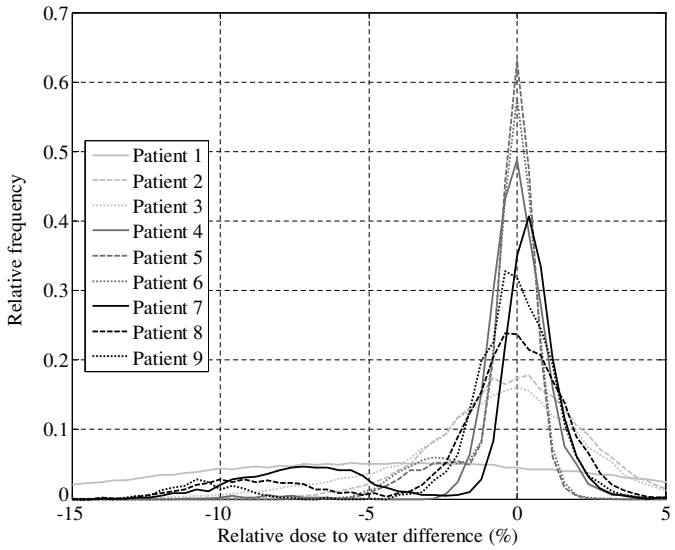

Figure 9. Histograms of the relative dose to water differences DD_{wat} (%) between the MC dose distributions D_{14wat} and D_{5wat}. D_{14wat} and D_{5wat} result from the conversion of D_{14} and D_5 from dose to medium to dose to water. Each histogram was plotted using a bin width of 0.4%.

Table 4. Dose to medium to dose to water conversion factors for the proposed CT conversion scheme of the Siemens Somatom Plus 4 CT scanner at Ghent University Hospital. The CT number interval and elemental composition corresponding to each material number are summarized in table 3.

Material number	Conversion factor
1	1.110
2	0.996
3	0.995
4	1.013
5	1.024
6	1.040
7	1.054
8	1.068
9	1.079
10	1.090
11	1.100
12	1.117
13	1.125
14	1.129

of the observed dose differences on the dose delivered to relevant structures it is best to look at DVHs. Figure 8(b) shows the DVHs of D_{14wat} and D_{5wat} for patient 3. The most apparent differences occur between the curves of both PTVs and the mandible. Note that—in contrast to figure 8(a)—D_{5wat} is higher than D_{14wat} within the bony structures. While the presence of soft bony tissues in the 14 bin CT conversion scheme increases the calculated dose to medium compared to the five bin CT conversion scheme because of the higher mass stopping power values, the DVHs change sides when the dose is converted to dose to water because the

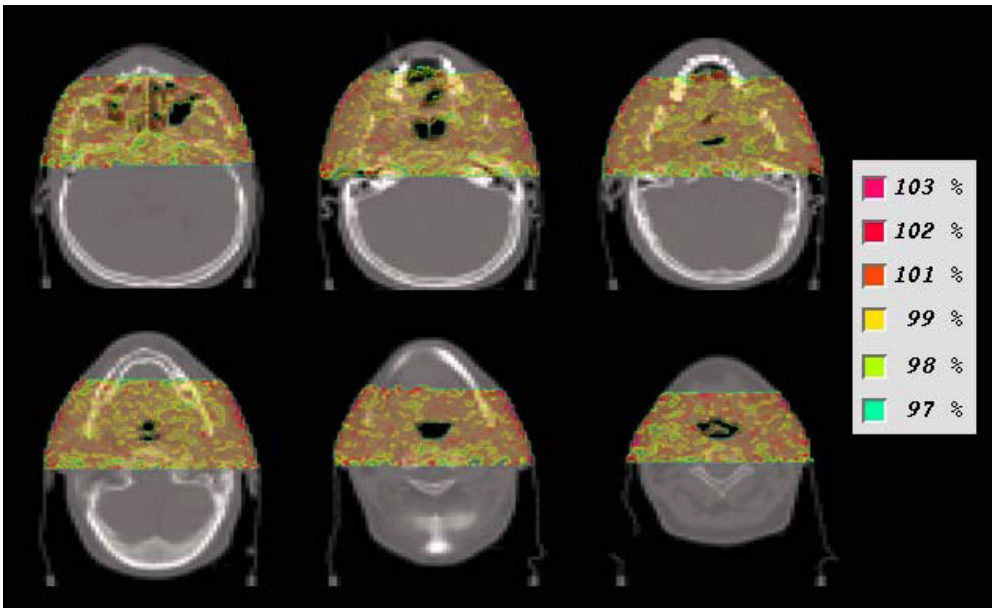

Figure 10. Isodifference plots showing values of 200% − D_A/D_B for several transversal slices for an oropharyngeal cancer patient case. D_A and D_B are the MC dose distributions calculated based on the CT conversion schemes of two different CT scanners. Values were only assigned to voxels that received more than 10% of the target prescription dose; voxels with a mass density value below 0.1 g cm^{-3} were not taken into account.

conversion factors for soft bony tissues are smaller. These opposite effects somewhat limit the observed dose to water differences between the 14 and five bin CT conversion schemes. Similar observations were made for the DVHs of bony structures within other patients. The largest difference was observed for patient 9, for whom the minimal dose received by 5% of the PTV volume was 10% higher for D_{5wat} than for D_{14wat}. It is thus highly important to use a CT conversion scheme that discriminates between different bone compositions when evaluating the dose to water.

With regard to the comparison of MC calculations using CT conversion schemes of different CT scanners, the dose difference distribution between D_A and D_B was calculated as 200% − D_A/D_B for each patient voxel. The results are shown in figure 10. It is clear that the differences are almost everywhere within 2% and mostly even within 1%. Despite the quite large difference of 268 HU between the calculated CT numbers of cortical bone for both CT calibrations (1535 HU for CT scanner A versus 1267 HU for CT scanner B), the influence on dose errors is apparently limited. This finding is in agreement with the statement of Constantinou *et al* (1992) that heterogeneity correction factors used by conventional dose engines for photon beam calculations are relatively insensitive to small changes in the CT number.

4. Conclusions

The conversion of CT numbers into material properties strongly influences the accuracy of patient dose calculations in Monte Carlo treatment planning. By studying the attenuation and energy deposition properties of human tissues as well as individual elements, we have shown

that it is particularly important to distinguish lung from air and different bone compositions from each other. The aim of our work was to develop a CT conversion scheme by performing a stoichiometric calibration of the CT scanner and by creating dosimetrically equivalent tissue subsets or bins. While each subset corresponds to a fixed material composition, the mass density could be calibrated continuously against the CT number. The proposed CT conversion scheme consisted of 14 bins: air, lung, adipose, muscle and ten bone bins. It was validated by performing MC calculations within virtual MC slab phantoms and within a real CT phantom containing different inserts. While the proposed CT conversion scheme was developed for a clinical 6 MV photon beam, it is also suitable for higher energy photons and for electrons.

The main focus of our work was to evaluate the proposed CT conversion scheme on patient treatment plans by means of a European multi-centre study. Nine patient cases with different tumour locations were selected. The proposed 14 bin CT conversion scheme was compared to a conventional five bin CT conversion scheme. The observed local relative differences in dose to medium were mostly smaller than 5%. The DVHs of the target and organs at risk were similar for both conversion schemes; only within certain bony structures D_{14} was found to be slightly but systematically higher than D_5. However, after converting the results to dose to water D_{5wat} became up to 10% higher than D_{14wat}. Indeed, the correction factor for cortical bone exceeds 1.10, while it only deviates a few % from 1 for soft bony tissues. It is clear that multiple bone bins need to be introduced when MC calculations of patient dose distributions are converted to dose to water. A comparison of the CT conversion schemes of different CT scanners showed that the influence of selecting the wrong conversion scheme is limited as the local dose to medium errors were below 2%.

Acknowledgments

Frank De Bisschop (Ghent University, Belgium) is acknowledged for preparing the $CaCl_2$ solutions. A Ferri and L Pierotti (Policlinico S.Orsola-Malpighi, Bologna, Italy) are acknowledged for their support with the Gammex RMI phantoms. Barbara Vanderstraeten is a Research Assistant (Aspirant) of the Fund for Scientific Research-Flanders (FWO-Vlaanderen).

Appendix. Stoichiometric calibration: fitting parameters

The stoichiometric calibration procedure of Schneider *et al* (1996) involves the determination of two parameters (K^{ph}/K^{KN} and K^{coh}/K^{KN}) through a least-squares fit of measured CT numbers to equations (1) and (2). In this way, however, negative K^{coh}/K^{KN} values were obtained for several CT scan protocols of our multi-centre study (table 2). Although the good quality of the fits based on these parameter values was shown in section 3.2, the occurrence of non-meaningful K^{coh}/K^{KN} values may indicate that the model of Schneider *et al* is overdetermined. Indeed, K^{ph}/K^{KN} and K^{coh}/K^{KN} are both functions of energy and are thus interrelated. The fits were repeated using this relationship instead of treating K^{ph}/K^{KN} and K^{coh}/K^{KN} as independent free parameters.

According to the parametrization of the total elemental attenuation coefficient by Rutherford *et al* (1976) (Schneider *et al* 1996, equation (7)), the ratio between K^{ph}/K^{KN} and K^{coh}/K^{KN} can be determined as follows:

$$\frac{K^{ph}/K^{KN}}{K^{coh}/K^{KN}} = \frac{(\mu/\rho)^{ph}}{(\mu/\rho)^{coh}} Z^{(1.86-3.62)}. \tag{A.1}$$

In this equation, $(\mu/\rho)^{\text{ph}}$ and $(\mu/\rho)^{\text{coh}}$ are the mass attenuation coefficients for photoelectric absorption and coherent scattering, respectively. While $K^{\text{ph}}/K^{\text{KN}}$ and $K^{\text{coh}}/K^{\text{KN}}$ are assumed to depend only on energy, the mass attenuation coefficients depend both on the element (Z) and energy. Values for $(\mu/\rho)^{\text{ph}}$ and $(\mu/\rho)^{\text{coh}}$ can be obtained as a function of photon energy from the NIST XCOM database (Hubbell and Seltzer 2004). Although the location-dependent energy spectrum of the CT scanner is unknown, an excellent linear relationship was obtained between the logarithms in base 10 of both parameters for the entire range of CT photon energies (20–120 keV). For oxygen (the most abundant element in human tissues) and calcium (the second most abundant element in cortical bone, after oxygen), respectively:

$$\text{O}: \quad \log\left(\frac{K^{\text{ph}}}{K^{\text{KN}}}\right) = 0.53\log\left(\frac{K^{\text{coh}}}{K^{\text{KN}}}\right) - 0.45 \quad (R^2 = 1.00) \tag{A.2}$$

$$\text{Ca}: \quad \log\left(\frac{K^{\text{ph}}}{K^{\text{KN}}}\right) = 0.54\log\left(\frac{K^{\text{coh}}}{K^{\text{KN}}}\right) - 0.51 \quad (R^2 = 1.00). \tag{A.3}$$

Clearly, the assumption that energy- and material-dependent factors can be separated is not entirely exact. Taking relationship (A.2) into account during the fit of measured CT data for the set of materials listed in table 1, resulted in values of $K^{\text{ph}}/K^{\text{KN}}$ and $K^{\text{coh}}/K^{\text{KN}}$ of 2.94×10^{-5} and 1.44×10^{-3}, respectively, for the Siemens Somatom Plus 4 CT scanner at GUH. Similarly, the use of (A.3) resulted in $K^{\text{ph}}/K^{\text{KN}}$ and $K^{\text{coh}}/K^{\text{KN}}$ values equal to 3.08×10^{-5} and 1.09×10^{-3}, respectively. The R^2-values of the fits based on (A.2) and (A.3) were both 0.998. The fits were thus hardly worse compared to the original fit ($R^2 = 0.999$), which treated $K^{\text{ph}}/K^{\text{KN}}$ and $K^{\text{coh}}/K^{\text{KN}}$ as independent free parameters.

Alternatively, the mass attenuation coefficient of a mixture can be calculated as the weighted sum of the coefficients of the constituent elements (Jackson and Hawkes 1981):

$$\left(\frac{\mu}{\rho}\right) = \sum_{i=1}^{n} w_i \left(\frac{\mu}{\rho}\right)_i. \tag{A.4}$$

For each element i, values of $(\mu/\rho)_i$ are available as a function of photon energy from the NIST XCOM database (Hubbell and Seltzer 2004). A quadratic fit can be performed through the 60, 80 and 100 keV data points. We assume that the unknown location-dependent energy spectrum of the CT scanner can be represented by a sole effective energy value E_{eff}. In this way, the CT number can be calculated as a function of E_{eff} through equations (A.4) and (2). The parametrization of the attenuation coefficient (1) is thus abandoned. The CT scanner can then be calibrated by determining the value of E_{eff} through a least-squares fit of measured against calculated CT numbers. As in the previous approach, only one fitting parameter is used. For the set of materials listed in table 1, this approach resulted in a value of E_{eff} equal to 73.0 keV, for the Siemens Somatom Plus 4 CT scanner at GUH. The R^2-value of the fit was 0.998.

In conclusion, in addition to the stoichiometric calibration procedure with two fitting parameters proposed by Schneider *et al* (1996), two alternative approaches were presented in this appendix. Both methods use only one fitting parameter, either $K^{\text{coh}}/K^{\text{KN}}$ or E_{eff}. By decreasing the number of independent fitting parameters, the unphysical negative $K^{\text{coh}}/K^{\text{KN}}$ values disappeared. For both alternative approaches, the quality of the stoichiometric calibration fit was hardly affected compared to the original two-parameter approach. However, both alternative methods require the use of experimental data from the NIST database. For the second alternative approach, fits of $(\mu/\rho)_i$ against E_{eff} had to be performed for all constituent elements of the calibration materials and human tissues, compared to only one fit of $K^{\text{ph}}/K^{\text{KN}}$

against K^{coh}/K^{KN} for the first alternative approach, thus introducing more uncertainty. On the other hand, the second alternative approach does not require the assumption that the mass attenuation coefficient can be parametrized by separating energy- and material-dependent factors. Throughout our paper, we have applied the original stoichiometric calibration procedure of Schneider *et al*, because it leads to very good results in practice. The occurrence of negative K^{coh}/K^{KN} values has no impact on our proposed CT conversion method.

References

Constantinou C, Harrington J C and DeWerd L A 1992 An electron density calibration phantom for CT-based treatment planning computers *Med. Phys.* **19** 325–7

de Kock E A and Schreuder A N 1996 Comments on 'The calibration of CT Hounsfield units for radiotherapy treatment planning' *Phys. Med. Biol.* **41** 1524–7

DeMarco J J, Solberg T D and Smathers J B 1998 A CT-based Monte Carlo simulation tool for dosimetry planning and analysis *Med. Phys.* **25** 1–11

du Plessis F C P, Willemse C A and Lötter M G 1998 The indirect use of CT numbers to establish material properties needed for Monte Carlo calculation of dose distributions in patients *Med. Phys.* **25** 1195–201

Fippel M 1999 Fast Monte Carlo dose calculations for photon beams based on the VMC electron algorithm *Med. Phys.* **26** 1466–75

Fippel M and Nuesslin F 2000 Comments on 'Converting absorbed dose to medium to absorbed dose to water for Monte Carlo based photon beam dose calculations' *Phys. Med. Biol.* **45** L17–8

Hartmann Siantar C L *et al* 1997 *Lawrence Livermore National Laboratory's PEREGRINE Project Report* UCRL-JC-126732

Hubbell J H and Seltzer S M 2004 *Tables of X-ray Mass Attenuation Coefficients and Mass Energy-Absorption Coefficients* (version 1.4) (Gaithersburg, MD: National Institute of Standards and Technology) http://physics.nist.gov/xaamdi (May 2006)

ICRU (International Commission on Radiation Units and Measurements) 1989 Tissue substitutes in radiation dosimetry and measurement *ICRU Report 44* (Washington, DC: ICRU)

Jackson D F and Hawkes D J 1981 X-ray attenuation coefficients of elements and mixtures *Phys. Rep.* **70** 169–233

Kawrakow I 2001 VMC++, electron and photon Monte Carlo calculations optimized for radiation treatment planning *Advanced Monte Carlo for Radiation Physics, Particle Transport Simulation and Applications: Proceedings of the Monte Carlo 2000 Meeting (Lisbon)* ed A Kling *et al* (Berlin: Springer) pp 229–36

Kawrakow I, Fippel M and Friedrich K 1996 3D electron dose calculations using a voxel based Monte Carlo algorithm (VMC) *Med. Phys.* **23** 445–57

Liu H H and Keall P 2002 D_m rather than D_w should be used in Monte Carlo treatment planning *Med. Phys.* **29** 922–4

Ma C M, Mok E, Kapur A, Pawlicki T, Findley D, Brain S, Forster K and Boyer A L 1999 Clinical implementation of a Monte Carlo treatment planning system *Med. Phys.* **26** 2133–43

Rogers D W O, Ma C M, Walters B, Ding G X, Sheikh-Bagheri D and Zang G 2002 *BEAMnrc User's Manual* (Ottawa: National Research Council of Canada)

Schneider U, Pedroni E and Lomax A 1996 The calibration of CT Hounsfield units for radiotherapy treatment planning *Phys. Med. Biol.* **41** 111–24

Schneider W, Bortfeld T and Schlegel W 2000 Correlation between CT numbers and tissue parameters needed for Monte Carlo simulations of clinical dose distributions *Phys. Med. Biol.* **45** 459–78

Seco J and Evans P M 2006 Assessing the effect of electron density in photon dose calculations *Med. Phys.* **33** 540–52

Siebers J V, Keall P J, Kim J and Mohan R 2000a Performance benchmarks of the MCV Monte Carlo system *13th Int. Conf. on the Use of Computers in Radiation Therapy (XIIIth ICCR)* ed W Schlegel and T Bortfeld (Heidelberg: Springer) pp 129–31

Siebers J V, Keall P J, Nahum A E and Mohan R 2000b Converting absorbed dose to medium to absorbed dose to water for Monte Carlo based photon beam dose calculations *Phys. Med. Biol.* **45** 983–95

Siebers J V, Keall P J, Nahum A E and Mohan R 2000c Reply to 'Comments on 'Converting absorbed dose to medium to absorbed dose to water for Monte Carlo based photon beam dose calculations'' *Phys. Med. Biol.* **45** L18–9

Van de Walle J, Martens C, Reynaert N, Palmans H, Coghe M, De Neve W, De Wagter C and Thierens H 2003 Monte Carlo model of the Elekta Sli*p*lus accelerator: validation of a new MLC component module in BEAM for a 6 MV beam *Phys. Med. Biol.* **48** 371–85

Verhaegen F and Devic S 2005 Sensitivity study for CT image use in Monte Carlo treatment planning *Phys. Med. Biol.* **50** 937–46

Wang L, Chui C S and Lovelock M 1998 A patient-specific Monte Carlo dose-calculation method for photon beams *Med. Phys.* **25** 867–78

Watanabe Y 1999 Derivation of linear attenuation coefficients from CT numbers for low-energy photons *Phys. Med. Biol* **44** 2201–11

White D R, Woodard H Q and Hammond M S 1987 Average soft-tissue and bone models for use in radiation dosimetry *Br. J. Radiol.* **60** 907–13

Woodard H Q and White D R 1986 The composition of body tissues *Br. J. Radiol.* **59** 1209–19